JPE 18-4-29

https://doi.org/10.6113/JPE.2018.18.4.1278
ISSN(Print): 1598-2092 / ISSN(Online): 2093-4718

Cross-Shaped Magnetic Coupling Structure for Electric Vehicle IPT Charging Systems

Siyuan Ren*, Chenyang Xia†, Limin Liu*, Xiaojie Wu*, and Qiang Yu*

†,*School of Electrical and Power Engineering, China University of Mining and Technology, Xuzhou, China

Abstract

Inductive power transfer (IPT) technology allows for charging of electric vehicles with security, convenience and efficiency. However, the IPT system performance is mainly affected by the magnetic coupling structure which is largely determined by the coupling coefficient. In order to get this applied to electric vehicle charging systems, the power pads should be able to transmit stronger power and be able to better sustain various forms of deviations in terms of vertical, horizontal direction and center rotation. Thus, a novel cross-shaped magnetic coupling structure for IPT charging systems is proposed. Then an optimal cross-shaped magnetic coupling structure by 3-D finite-element analysis software is obtained. At marking locations with average parking capacity and no electronic device support, a prototype of a 720*720mm cross-shaped pad is made to transmit 5kW power at a 200mm air gap, providing a 1.54m^2 full-power free charging zone. Finally, the leakage magnetic flux density is measured. It indicates that the proposed cross-shaped pad can meet the requirements of the International Commission on Non-Ionizing Radiation Protection (ICNIRP) according to the Australian Radiation Protection and Nuclear Safety Agency (ARPANSA).

Key words: 3-D finite-element analysis, Cross-shaped magnetic coupling structure, Inductive power transfer, Leakage magnetic flux density

I. INTRODUCTION

Based on Ampere's and Faraday's Laws, inductive power transfer (IPT) uses an alternating magnetic field to transfer power across an air gap without physical contact. The electrically isolated components contribute to its inherent advantages. In addition, operation in wet environment does not introduce any potential risks. Over the last decade, IPT technology has become a major focus for research since MIT made breakthroughs in its development. Nowadays, IPT has been applied in numerous fields such as mobile phones [1], [2], medical facilities [3], [4], household appliances [5], and especially in transportation including buses [6], automatic guided vehicles (AGVs) [7] and electric vehicles (EVs) [8]-[10].

IPT systems are generally grouped into online and static depending on whether or not there is relative motion between the transmitter and receiver pad of the magnetic coupling structure. The transmitter pad is often used for continuous power supply to vehicles in motion, while the receiver is applied to charge plug-in batteries after parking in a fixed position. Due to the high distance of the primary track, the coupling coefficient of an online IPT system is low. According to the coupling coefficient, static IPT systems are subdivided into two types: loose coupling and close coupling. Close coupling generally requires inserting a charging paddle into a port. The small air gap enables high energy density transition in a relatively small volume [11]. For loose coupling, where the transmitter and receiver are placed in parallel and have a relatively large air gap, automatic power transfer can be performed. Therefore, it is widely accepted as the most suitable IPT system for EVs, and is the subject of this paper as well.

The magnetic coupling structure is the characteristic component that directly determines the system capability. The parameter which can effectively evaluate the magnetic coupling structure is the coupling coefficient k. Due to a large air gap, the numerical range of the typical IPT system coefficient is 0.01-0.5, which poses limitations on the output power (0.5W-50kW) [12]. In terms of the IPT systems of

Manuscript received Sep. 21, 2017; accepted Mar. 1, 2018
Recommended for publication by Associate Editor Honnyong Cha.
†Corresponding Author: 18260722082@163.com
Tel: +86-0516-83885667, Fax: +86-0516-83885667, China University Mining and Technology
*School of Electrical and Power Engineering, China University of Mining and Technology

EVs, the application is often confined due to custom differences in drivers that lead to a distance shift between transmitter and receiver of the power pad. As a practical solution, the circular electromagnetic coupling structure is further improved to have a higher coupling coefficient and better shifting features. The diameter of a circular pad needs to be increased significantly to achieve good coupling for the charging performance of EV IPT systems [13]. In addition, a number of magnetic coupling structures have been proposed. A new IPT structure for EV wireless charging systems has been designed and flux pipes were introduced [14]. A flux pipe is channeled by a coil array design along a maximum length of ferrite to increase the path height as well as to minimize inductance. Two coils are magnetically in series (flux from one coil passes through the other) while electrically they are in parallel and are required to reduce inductance by the power supply. However, the flux pipe produces a front and a back branch, and the flux passes similarly through both of them. Based on this assumption, the leakage induction is considerable, and correspondingly a polarized single-sided flux structure is proposed [12]. It is referred to as a double D (DD) structure due to the pair of symmetrically connected "D" shapes. When compared to circular magnetic coupling structures, the double D has a higher coupling coefficient and better horizontal offset tolerance in the vertical direction of the ferrite stripes. When compared to the new IPT magnetic coupling structure [14], only upward single-sided flux is produced in the double D structures, which increases the main flux of the transmitter and receiver pad and decreasing the leakage flux. The double D structure has become a magnetic structure applied in electrical vehicle wireless charging since it combines the advantages of both circular pads and the flux pipe structures [10], [24]. Later, a number of electromagnetic coupling structures, including DDQ, BBP, etc., were proposed based on DD pads [15], [16]. These structures can solve the problem of an undesired shifting features along the ferrite bar direction to some extent. However, the added copper increases manufacturing and running costs (copper loss). In addition, they cannot overcome the principal weakness of centered revolution deviations of DD coils, which requires no angular shift between the transmitter and receiver in the charging zone for EVs. As a result, the charge performance is reduced sharply. Such restrictions pose high limitations on free parking and charging efficiency.

This papers proposes a novel magnetic coupling structure for EV wireless charging systems, which is referred to as cross-shaped pads. To have an efficient design, 3-D magnetic field finite element analysis (FEA) software is used for the optimization of its ferrites structures, coil shapes and turns. When compared with DD pads and square pads, the magnetic structures in EV wireless charge standards SAE TIR J2954, the proposed crossed-shaped pads have desirable horizontal shifting tolerance and centered resolution characteristics. Finally, the proposed device is shown to stably transmit a 5kW output power with a converter to charge EV batteries at a 200mm distance. In experiment, a 1.54m^2 circular full-power free charging zone satisfies the requirements of manual parking. Finally, the leakage magnetic flux density is investigated for EV IPT charging systems.

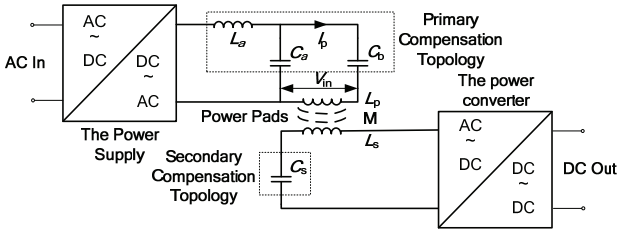

Fig. 1. IPT system components.

II. IPT SYSTEMS

A typical IPT system mainly consists of a power supply, a primary compensation topology, power pads, secondary compensation topology and a power converter, as shown in Fig. 1. The power supply generates a sinusoidal current (typically between 20 kHz and 100 kHz) to motivate the transmitter of the power pad to generate a magnetic field that emits power at a same frequency as the excitation current. Then the PU pad receives and transforms the magnetic energy into electrical power. Finally, the load obtains energy from the power converter. Both the transmitter pad and the PU pad make up a magnetic coupling structure, which is the focus of this article. At the same time, to minimize the reactive power of the whole system and to make the power supply work under the soft-switching condition, primary and secondary compensation topology is needs to match the impedance with the transmitter pad and the PU pad at the operation frequency.

The LCC compensation network structure is adopted at the primary and S compensation is adopted at the secondary. This enables independence between the original track of the circuit and the load in a simple control circuit. Meanwhile the magnetic and electrical design can be separated, reducing design complexity.

The output power (P_{out}) of an IPT system can be expressed as a product of the open circuit voltage (V_{oc}), short circuit current (I_{sc}) and load-dependent quality factor (Q_s) as shown in equation (1).

$$P_{out} = P_{su}Q_s = V_{oc}I_{sc}Q_s = \omega {I_p}^2 \frac{M^2}{L_s}Q_s = V_{in}I_p k^2 Q_s \quad (1)$$

where P_{su} is the output power of an IPT system without the secondary component topology, which is also equal to the product of V_{oc} and I_{sc}; ω is the frequency of the operation; I_p is the current flowing through the transmitter pad; V_{in} is the voltage across the transmitter pad; M, L_s and k represent the

mutual inductance between the power pads, the self-inductance of the PU pad when the transmitter pad is an open circuit and the coupling coefficient of the power pads, respectively. From equation (1), it can be concluded that the output power of the system is determined by the VA at the input terminal of the transmitter pad ($V_{in}I_p$), the transformer coupling coefficient (k) and the load-dependent quality factor Q_s [18]. The VA rating of the transmitter pad is limited by the voltage across the transmitter pad (V_{in}) and the current inside (I_p). However, both of them have to be balanced against electrical insulation class and the copper loss of the transmitter pad. In engineering experiments, due to the ratings and tolerances of the component VA, Q_s is limited to between 2 to 10 [19]. The ratio between the magnetic flux through the power pads and the total flux produced by the transmitter pad is defined as the coupling coefficient k. This is beneficial for comparing the magnetic properties of different power pads. The coupling coefficient k, depending on the distance between the transmitter pad and the PU pad, is expected to be higher to ensure the overall efficiency, feasibility and cost effectiveness of the IPT system.

III. Proposed Magnetic Coupling Structure

The magnetic coupling structure plays a leading role in IPT systems, where the air gap is fairly large between power pads and the energy required for transmission is stronger.

Therefore, ferrite cores should be used to improve the coupling coefficient and electromagnetic capacity. Pot [20], U [21], and E cores [22], [23] are often seen in addition to the most commonly used "I" core [12]-[16]. In this paper, a novel IPT magnetic coupling structure consisting of two rectangular coils and ferrites is proposed as shown in Fig. 2. The two rectangular coils are spatially orthogonal. They are referred to as the cross-shaped magnetic coupling structure or cross-shaped pads. The coils are placed up next to the rectangular ferrites snugly, which regulates the flux paths. There is no MMF (magneto motive force) being produced that can drive the flux out the back. The shaded portion of the coils and ferrites in Fig. 2 indicates some flux pipes since the coils are magnetically in series and electrically in parallel.

In order to further study the cross-shaped pads, 3-D finite-element analysis software ANSYS Maxwell, which was used in [12]-[14], has been utilized. Meanwhile, a large number of verification experiments are carried out. To illustrate the performance of cross-shaped pads, an arbitrary cross-shaped pads prototype with the same transmitter pad and receiver pad is established in Maxwell as shown in Fig. 3(a). Fig. 3(b) shows the magnetic force lines distribution of a cross section of AA'C'C of the cross-shaped pads shown in Fig. 3(a), where Φ_0 is the main magnetic flux, while Φ_1 and Φ_2 are the leakage magnetic flux. The flux pipes shown in Fig. 2 can emit magnetic force lines farther, which increases Φ_0 and decreases Φ_1 and Φ_2 to improve the performance of the power

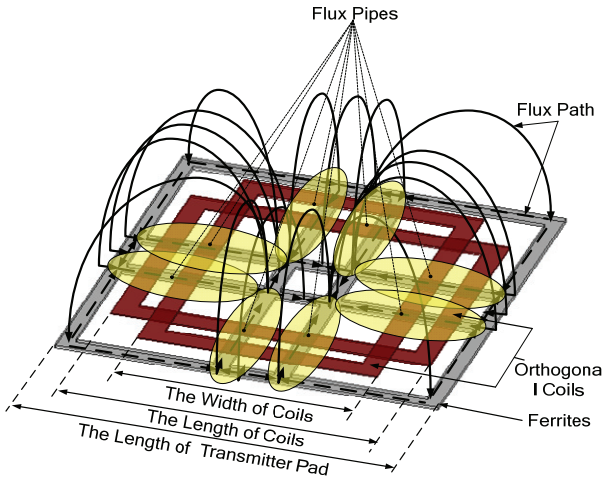

Fig. 2. Magnetic force line distribution of a cross-shaped pad.

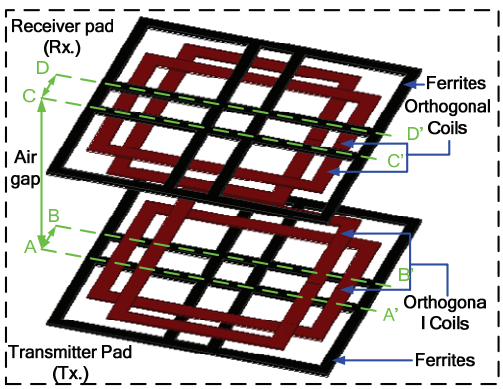

(a)

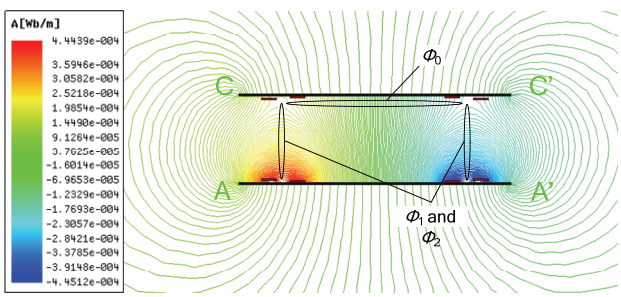

(b)

Fig. 3. Schematic diagram of cross-shaped pads.

pads. The improvement effect of the eight flux pipes is obvious to see.

Some simplifications are made for this simulation model. For instance, a compromise between the size of the surrounding air region and elements has been made to achieve the highest accuracy in terms of the simulation time ratio. However, in practice, wire has a minimum bending radius so that the coils are constructed with rounded corners. For simulation purposes, square corners are used to reduce the model complexity. Manufacturing tolerances result in imprecise positions of the coils and ferrites, which influences the accuracy to a small but acceptable extent.

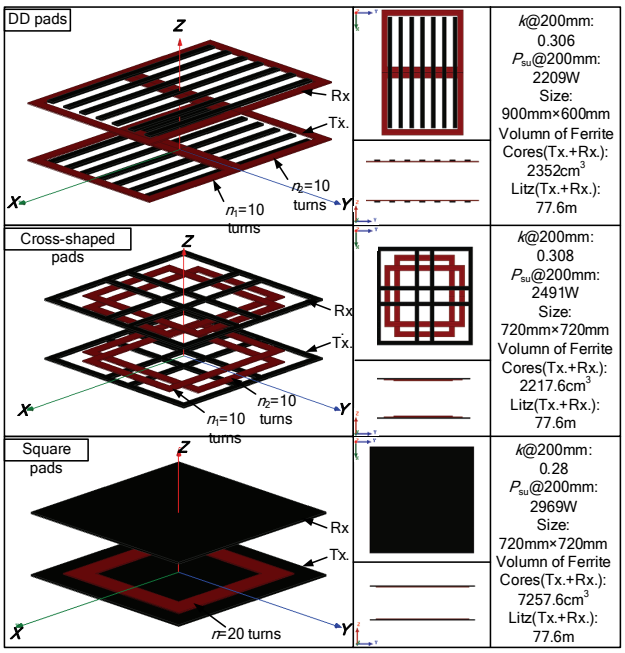

Fig. 4. Comparison of DD pads, square pads and cross-shaped pads.

To fully show the characteristics of cross-shaped pads, existent magnetic topologies are compared. According to EV wireless charging standard SAE TIR J2954, a couple of magnetic path topologies including square and DD are chosen as alternatives under the same air gap (200mm), the same Litz wire length (77.6m) and the same ferrite thickness (7mm). Fig. 4 shows that the needed magnetic core volume and cross section area of crossed-shaped pads is lower than that of DD pads. In addition, the coupling coefficient k=0.308 is equal to that of DD pads and higher than that of square pads. In order to further compare DD pads, square pads and cross-shaped pads, some offset characteristics under the condition shown in Fig. 4 have been studied and shown in Fig. 5. In this paper, "horizontal offset" describes the distance between the pad centers in the X-axis or Y-axis direction, "vertical offset" describes the distance between the pad centers in the Z direction, while "center rotation offset" describes the angle of rotation around the Z-axis.

The three offsets in Fig. 5 show a number of things. (a) The vertical tolerance of DD and cross-shaped pads is superior to that of square pads. (b) The horizontal Y-direction shifting tolerance of DD pads is superior to that of X. Both the cross-shaped and square pads are center symmetrical. Therefore, there is only one shifting curve horizontally. The horizontal Y-direction shifting tolerance of cross-shaped pads is superior to the X-direction of DD pads. However, it is inferior to the Y-direction of DD pads and square pads. (c) The centered resolution shifting tolerance of cross-shaped pads is the highest, with performances where the coupling coefficient k always remains the maximum, and remains the minimum fluctuation of the coupling coefficient k of the

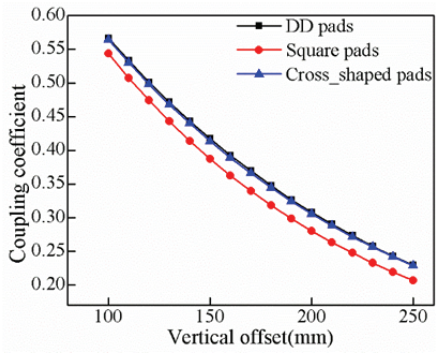

(a)

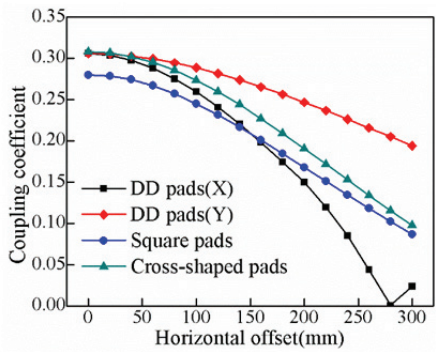

(b)

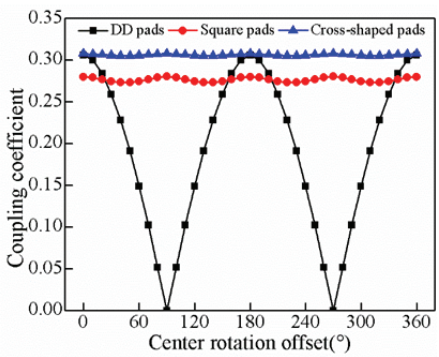

(c)

Fig. 5. Coupling coefficient comparison of various offset characteristics of DD pads, square pads and cross-shaped pads under the conditions shown in Fig. 4: (a) Vertical offset; (b) Horizontal offset at a gap of 200 mm; (c) Centered rotation offset at a gap of 200 mm.

shifting angle variation that axially revolves. The curve fluctuation of DD pads is reduced to 0 at 90° and 270°. This has a fatally detrimental effect on wireless charging systems.

Interoperability is very important for EV applications. The transmitter and receiver side of a WPT system may or not be produced by the same manufacturer. Therefore, cross-shaped pads are set as the generation for power pads. The three structures of DD, square and cross-shaped, shown in Fig. 4, are selected as receivers and compared under horizontal shift conditions. Fig. 6 shows that the power pads achieved a desired match when both the emitter and receiver are cross-shaped while interoperability between cross-shaped and square is possible. However, the crossed-shaped/DD pair has

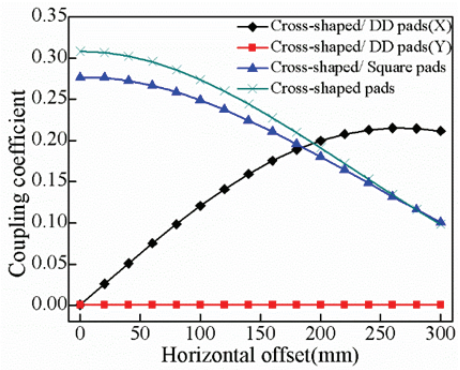

Fig. 6. Interoperability comparison of different constitutes.

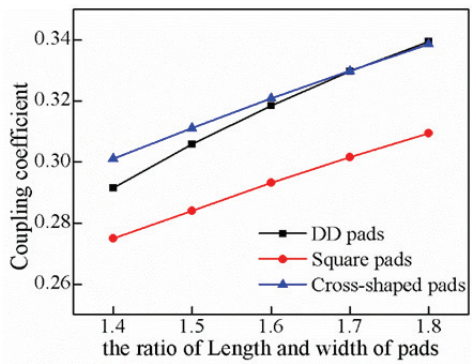

Fig. 7. Coupling coefficients of DD pads, square pads and cross-shaped pads as j varies from 1.4 to 1.8, under the conditions of identical pad sectional area, air gap distance, ferrite thickness and Litz wire.

almost 0 coupling coefficient at full alignment, and the value remain unchanged with distance increase along the Y-axis, while it rises first and then drops with distance decrease along the Y-axis. Therefore, both structures need improvement that can be realized by increasing the Q-coils. By evaluating the crossed-shaped/square pads pair and the crossed-shaped/DD pads pair, it is assumed that the crossed-shaped and DDQ have the desired interoperability.

It is known that for DD pads, a higher length of a couple of sides with a reasonable range is desired. The analyzed DD pads have a length-to-width ratio of 1.5 (900mm/600mm). To have a more comprehensive comparison of the three magnetic structures, in following the ratio of DD pads, j varies by 1.4-1.8, with the air gap remaining at 200mm. In addition, there is a guarantee of identical cross sectional areas, ferrite thicknesses and lengths of Litz wire for the three pads. A variation curve of the coupling coefficient k is shown in Fig. 7. The values of the cross-shaped and DD are higher than those of the square. When j<1.7, the coefficient of the cross-shaped is higher than the DD, while not being discriminable when j>1.7. This is because the ferrite volume of the DD is always higher than that of the cross-shaped. In addition, the volume increases with a higher j value.

Cross-shaped pads are a new kind of electromagnetic coupling mechanism with a higher coupling coefficient and higher tolerances in terms of the vertical and center rotation offsets. This contributes to multiple flux paths in the cross-shaped pad that can to a large extent intensify the main flux between the primary launch side and the secondary pick-up side.

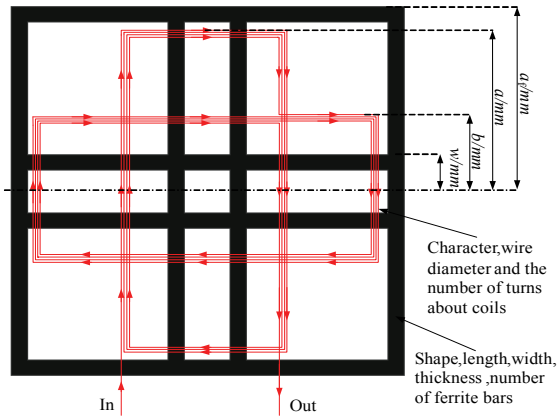

Fig. 8. Wire running method and major design variables of a cross-shaped pad.

IV. Design and Optimization of Cross-Shaped Pads

A. Modelling the Power Pads

IPT systems and cross-shaped pads magnetic circuit principles are introduced in Section II and Section III. A comparison of cross-shaped pads, square pads and DD pads shows that the cross-shaped pads deserves further research. Therefore, in this section, the task is to design and optimize the cross-shaped pads for better capability when a large number of design parameters is changed as shown in Fig. 8. These parameters include the shape, length, width, thickness and number of ferrite bars. They also include the character, wire diameter and number of turns of the coils, along with the width of the coils, length of the coils and so on. It is impractical to deal with all of these. Therefore, the investigation is narrowed in scope based on experience and existing research. For example, in order to balance the coils copper loss and the transmitted energy of the power pads, the effective value of the excitation sinusoidal current is set to 20A (f=20kHz). The expected shape of the ferrite strips is made of readily available "I" core of 30mm in width, which is enough to channel magnetic flux. The Litz wire of orthogonal coils is about 4mm in diameter and it is made of enameled wire (0.1mm×800). For the transmitter pad, the edge length of the ferrite strips is $2a_f$, the length of coils is $2a$, the width of coils is $2b$, the spacing of middle ferrite strips is $2w$ and turns for each of the rectangular coils are n as shown in Fig. 8. Several variables are defined for a detailed analysis of cross-shaped pads, where the ratio of a_f and a is referred to as v, the ratio of w and a is referred to as c, and the ratio of b and a is q. The receiver pad is identical to the transmitter pad.

Ferrites shapes		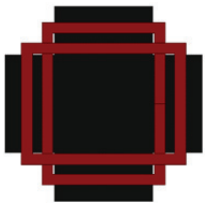			
Identifier	(a)	(b)	(c)	(d)	(e)
k(at given separation)	0.589(100mm) 0.429(150mm) 0.315(200mm) 0.234(250mm)	0.556(100mm) 0.399(150mm) 0.289(200mm) 0.213(250mm)	0.571(100mm) 0.418(150mm) 0.308(200mm) 0.229(250mm)	0.567(100mm) 0.417(150mm) 0.308(200mm) 0.230(250mm)	0.530(100mm) 0.389(150mm) 0.288(200mm) 0.215(250mm)
Volume of ferrites(cm^3)	7257.6	5443.2	3175.2	2217.6	1705.2

Fig. 9. Comparison of different ferrite shapes.

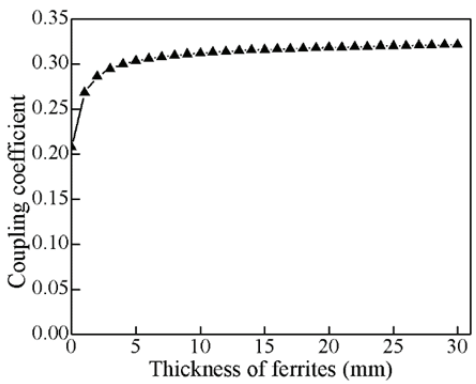

Fig. 10. Coupling coefficient variation of cross-shaped pads as the thickness of their ferrite strips varies from 0mm to 30mm.

B. Shapes of Ferrite Strips

In order to optimize performance, ferrite strip shape is obtained when a is 300mm, v is 1.2, q is 0.75, the thickness of the ferrites is 7mm and the turns of each coil are 10. Some of the different shapes of ferrite strips that constitute cross-shaped pads are shown in Fig. 9. The profiles of these power pads have been compared and the results of the coupling coefficient of different pads at 100mm, 150mm, 200mm and 250mm are shown in the descending order of the volume of the ferrite cores.

In practical applications, separation ranging 100mm-250mm is enough for the IPT systems of EVs. Among Fig. 9(a)-(e), the coupling coefficients in (b) and (e) are lower. The coefficients in (a) are slightly higher than those in (c) and (d). However, the ferrite volume used is 2.3 times that of (c) and 3.3 times that of (d). The coefficients in (c) and (d) are basically identical, and the volume in (d) is only 70% of the volume of (c). Therefore, it is not very good for the coupling coefficient that the volume of the ferrites is used, and the ferrites should be arranged reasonably to improve the flux path. In the end, (d) is chosen as the ferrite structure used in cross-shaped pads.

C. Thickness of Ferrite Strips

It is shown in Fig. 10 that the ferrites thickness is 0mm, which corresponds to a very low coupling coefficient. Therefore, it is critical to add-in a ferrite structure. However, the ferrite thickness >5mm has little impact on the coupling coefficient k, since a further increased value will not affect the magnetic flux path when the excitation current remains unchanged. With a lower thickness value, an increase in the value can reduce the magnetic resistance. However, when the value has been reached to some extent, the reduced resistance is fixed and no longer affected.

However, the thickness value can affect the flux density, which can result in magnetic damage. Fig. 11 shows the flux density distribution at the values of 7mm, 14mm, 21mm and 28mm. The maximum core flux density value is obtained and it is reduced with an increase in the ferrite thickness. Therefore, excess ferrite results in high cost and weight, while insufficiency ferrite can result in magnetic saturation. Hence, optimization regulation is to reduce the thickness under the condition of no excess of the saturation limit with the margin considered. Based on experiments and manufacturing conditions, 20mm is selected for the simulation and experimental verifications. The material properties includes relative permeability 2500, Curie temperature 215℃ and saturation flux density 380mT at 100℃.

D. Edge Length of the Ferrite Strips

The edge length of ferrite strips is a key parameter in terms of the performance of cross-shaped pads. Therefore, it is necessary to investigate its influence on the coupling coefficient by a_f or $v(a_f/a)$. Fig. 12 shows the relationship between the coupling coefficients under various a-values of the cross-shaped pads and the ratio v. This demonstrates that by increasing v, the coefficient k is increased. However, this tendency is reduced under different coil dimensions. Fig. 13 shows that the coupling coefficient under different v ratios

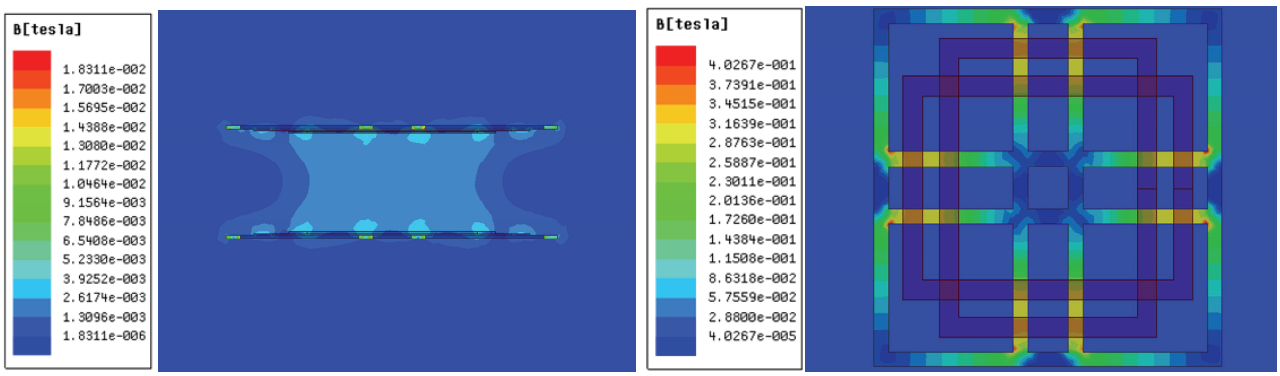

(a)

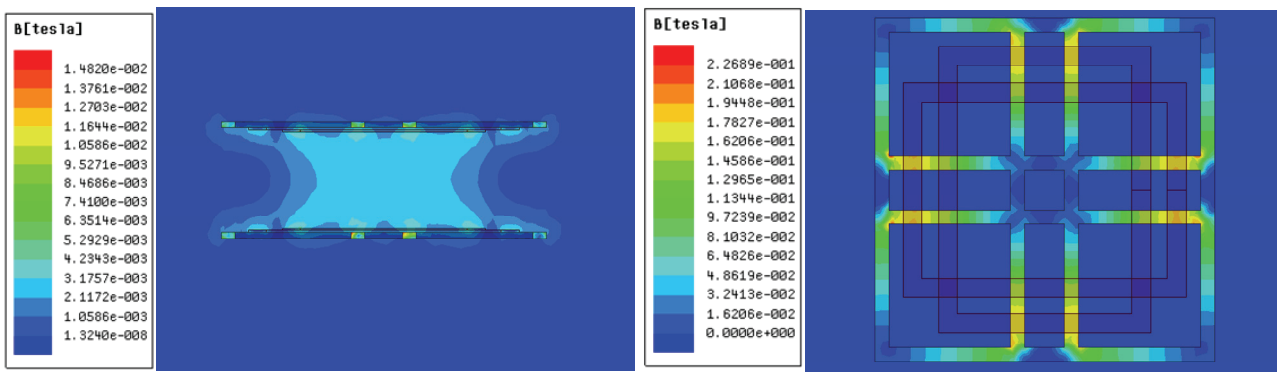

(b)

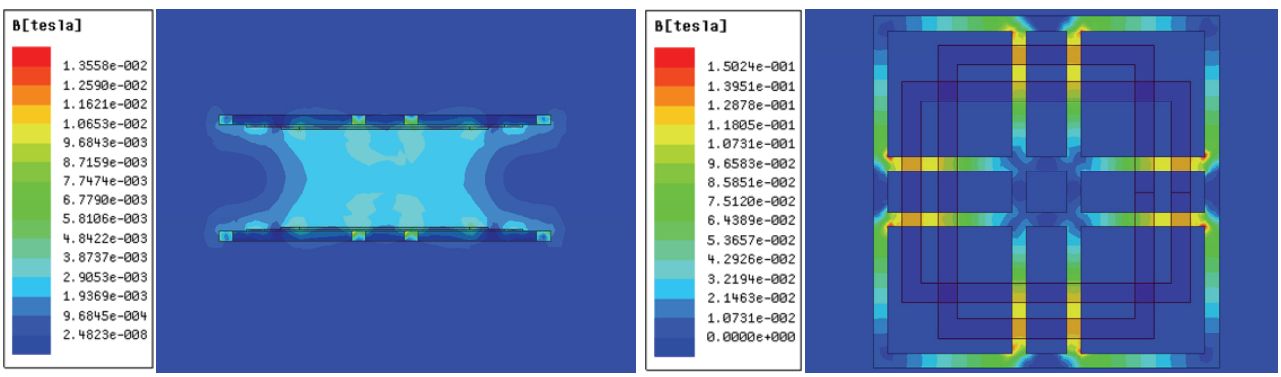

(c)

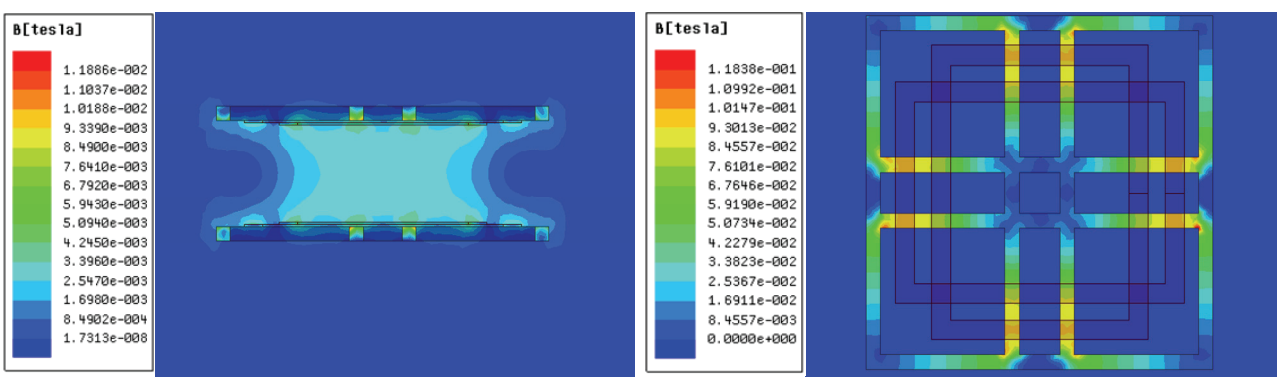

(d)

Fig. 11. Magnetic flux density simulation diagrams with the same primary excitation current and the secondary pick-up current of the 20 arms at 20 kHz under different ferrite thickness values: (a) 7mm; (b) 14mm; (c) 21mm; (d) 28mm.

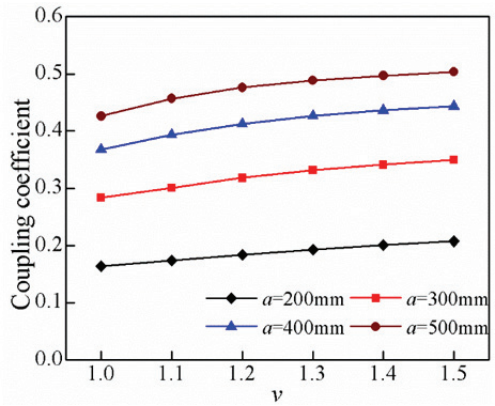

Fig. 12. Coupling coefficient k as v varies from 1 to 1.5 (q=0.75, c=0.2 and n=10).

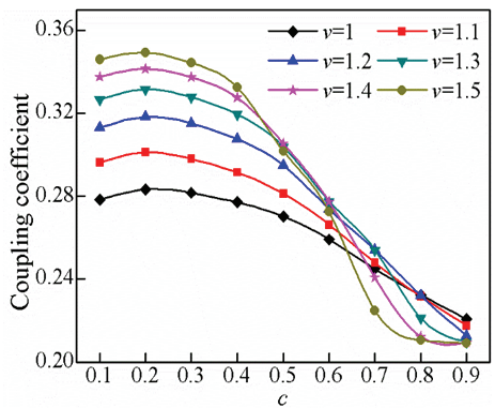

Fig. 13. Coupling coefficient k as c varies from 0.1 to 0.9 (a=300mm, q=0.75 and n=10).

takes up uniformity, with the ratio c steadily increasing. First it goes up and then down, with local extremes at c=0.2. Meanwhile at c=0.2 the coefficient k rises up with an increase of v. Therefore, the value of a_f can be determined by the constraint geometry of the actual pads and the parameter a.

E. Spacing between Ferrite Strips

An optimization analysis of the shapes of ferrite strips was made in the previous section, and the optimal solution is shown in Fig. 9(d). Fig. 13 shows a potential optimum value of the ratio c. Therefore, the spacing between the middle ferrite strips should be optimized in the case of a constant volume. In this paper, the optimal ratio c is determined. Fig. 14 shows variation curves of the coupling coefficient k in terms of variation of c under different parameters.

Fig. 14(a) shows that the coupling coefficient k increases gradually with an increase of a, which is expected of a value as high possible for practical applications. The value of k increases at first and then decease as c varies from 0.1 to 0.9. The value of k obtains its optimal value when c is 0.2, regardless of the value of a. All of the results of the analysis in this paragraph are under the conditions that q is equal to

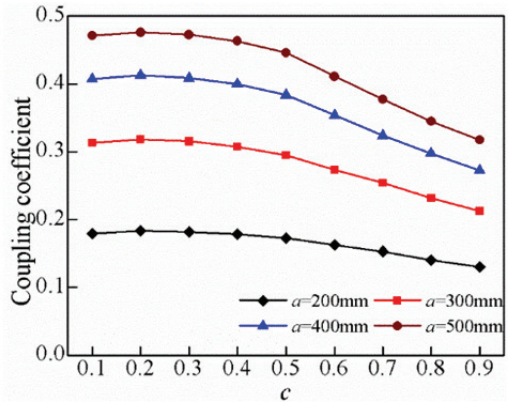

(a)

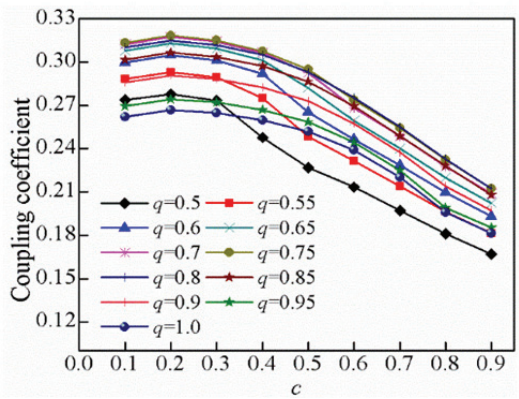

(b)

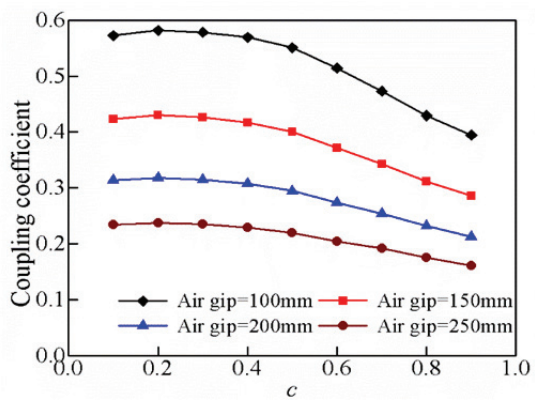

(c)

Fig. 14. Coupling coefficient k as c varies from 0.1 to 0.9 at the different values of: (a) a (v=1.2, q=0.75, air gap = 200mm and n=10); (b) q (a=300mm, v=1.2, air gap = 200mm and n=10); (c) air gap (a=300mm, v=1.2, q=0.75 and n=10).

0.75 and the air gap is 200mm, which means the results are unrepresentative. The next step is to research the coupling coefficient as c varies from 0.1 to 0.9 at different values of q and the air gap as shown in Fig. 14(b) and 14(c), respectively. Results show that c=0.2 is independent of the optimal solution of q and the air gap. Therefore, through the above analysis, the optimal layout for the ferrite strips of power pads is shown in Fig. 15, where the length of the ferrite strips is $2a_f$, and w is equal to $0.2a$.

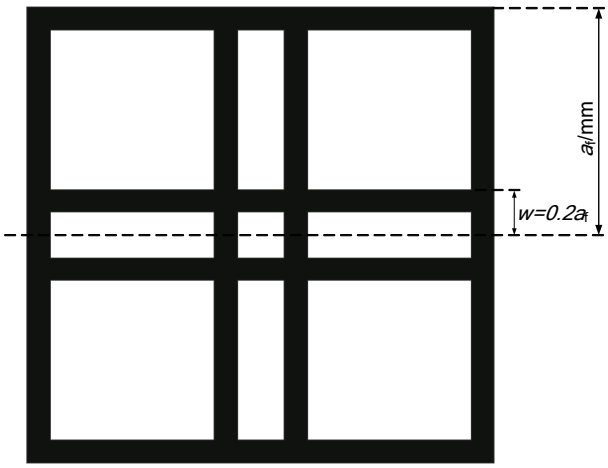

Fig. 15. Optimal ferrite strips of power pads.

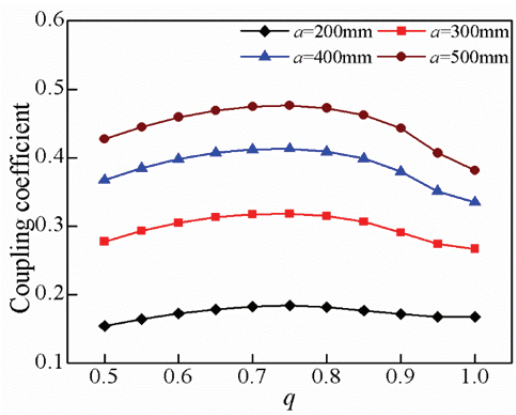

(a)

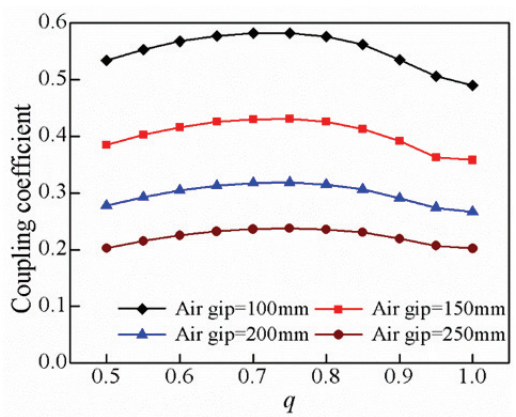

(b)

Fig. 16. Coupling coefficient k as q varies from 0.5 to 1 with the optimal ferrite strips at different values of: (a) a (v=1.2, air gap is 200mm and the turns of each coil is 10); (b) Air gap (a=300mm, v=1.2 and the turns of each coil is 10).

F. Length and Width of Coils

The optimal ferrite strips for power pads are shown in Fig. 15. In this part, the length and width of the orthogonal coils are researched for achieving a greater coupling coefficient k. The curves of the coupling coefficient k are shown in Fig. 16 when q varies from 0.5 to 1 with the optimal ferrite strips at different values of a and air gap.

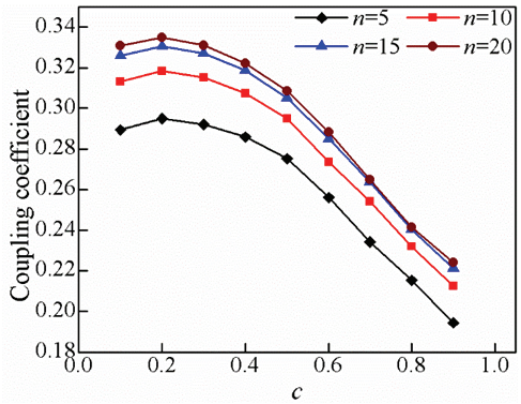

(a)

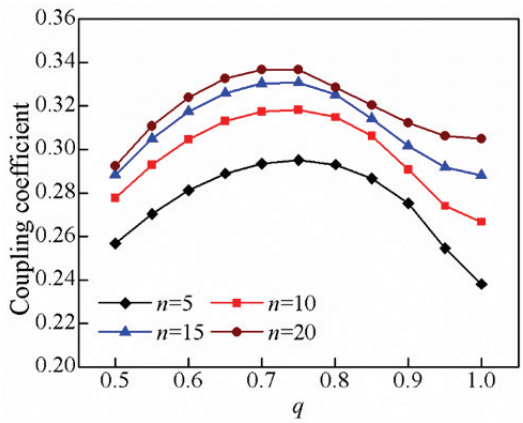

(b)

Fig. 17. Influences of the turns for each of the rectangular coils n with different optimal parameters: (a) Coupling coefficient k as c varies from 0.1 to 0.9; (b) Coupling coefficient k as q varies from 0.5 to 1 with optimal ferrite strips (a=300mm, v=1.2 and air gap =200mm).

Fig. 16(a) shows that coupling coefficient k is monotonically increasing with an increase of a. First it increases then it deceases with q=[0.5, 1]. Thus, the optimal a should be as high as possible to adjust to practical application. The optimized q for the coupling coefficient of cross-shaped pads is obtained when q=0.75. An analysis of the influence of different air gaps on the optimal value of q for a higher coupling coefficient k is shown in Fig. 16(b). It can be seen that there is no difference in the optimized q value when the air gap of power pads varies from 100mm to 250mm.

G. Turns of Coils

All of the previous analyses are in the case where the number of turns of each rectangular coil is n=10. The parameter n ranging from 5-20 is studied considering the energy transfer of the system and the safety voltage levels of the windings. In this part, the variation of n on different optimal parameters is shown in Fig. 17. The curves in Fig. 17(a)-(b) show that an n variation within 5-20 does not affect

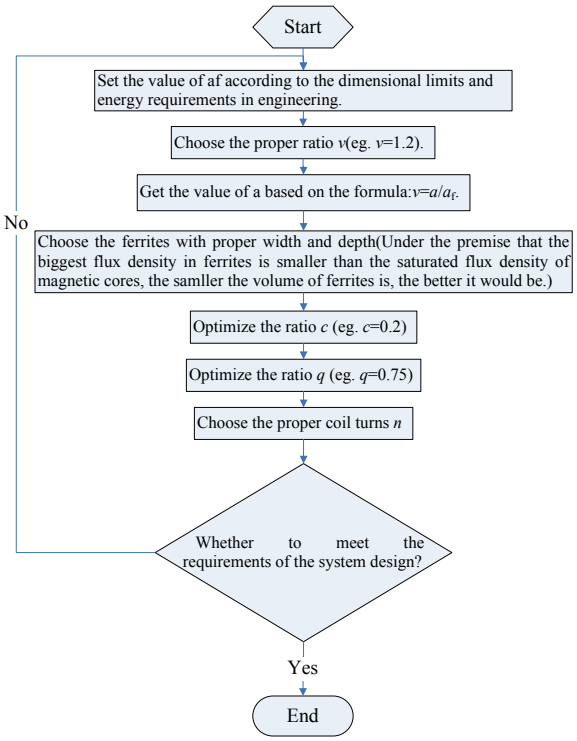

Fig. 18. Flow diagram for the design of cross-shaped pads.

the optimization mentioned above.

In summary, if cross-shaped pads are chosen to be the power pads of an IPT system, the flow diagram of Fig. 18 can be used as a reference.

V. Implementation of Cross-Shaped Pads

To demonstrate the proposed cross-shaped pads, a prototype of these pads in a 5kW IPT system has been built as shown in Fig. 19. Considering the inherent limitations of EVs, a= 300mm, v=1.2, c=0.2, q=0.75 and n=10 have been selected. They have been analyzed and optimized in Section VI.

With the schematic diagram in Fig. 1, a 5kW test bench is built up and shown in Fig. 19. Some of the experiment parameters is listed in Table I and some of the key values are in Table II. In addition, L_a, L_P, L_S, C_a, C_b and C_S are demonstrated in Fig. 1. f is the working frequency, U_{DC} is the DC input voltage of the inverter, I_P is the coil current of the emitter pad, U_L, I_L and P_{out} are the DC output voltage, the current effective value and the output power, respectively. The output inverter voltage $u_{DC\text{-}AC}$, the launch pad current i_P of the primary side as well as the waveforms regarding the system output voltage U_L and current I_L when the power pads are totally aligned are shown in Fig. 20, which illustrates a capacity of 5kW.

In Fig. 20(a), the phase lag of i_P to $u_{DC\text{-}AC}$ is 90°. In addition, the value of i_P do not change since the coupling coefficient changes[8]. Therefore, when the electromagnetic coupling mechanism shifts, the loss of the primary-side transmitting

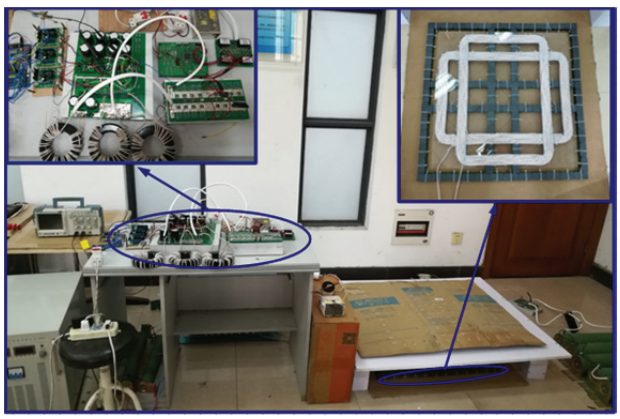

Fig. 19. 5kW test bench.

TABLE I
Experimental System Parameter Values

Parameters	Values
L_a	125.3μH
L_P	466.3μH
L_S	465.12μH
C_a	0.51μF
C_b	0.18μF
C_S	0.14μF

TABLE II
Key Values of the System Parameters

Parameters	Values
F	20kHz
U_{DC}	350V
I_P	19.9A
U_L	390.6V
I_L	12.9A
P_{out}	5039W

coil is basically fixed. However, in Fig. 20(b), the value of U_L will decrease as the coupling coefficient decreases. The value of I_L has to be increased in order to keep the system output power invariant. However, this causes a decrease in the whole system efficiency.

The quality of the IPT system is determined by the power pads, while the pads are either standing or lying which is determined by the coupling coefficient k and its load-dependent quality factor Q_s. The factor is the ratio of the inductive impedance to the resistance at the operational frequency ($Q_s=\omega L/R$), which also represents a quality indicator of the ratio of the energy stored in the inductance coil to the energy lost in each cycle at the working frequency. The coupling coefficient of the prototype, as shown in Fig. 19, significantly decreases with an increase of the air gap, which is shown in Fig. 21(a). Considering the relative position of the vehicle chassis and the ground, a 200mm air gap is selected to study the performance of the cross-shaped pads prototype. The transmitter pad of the prototype has a Q of

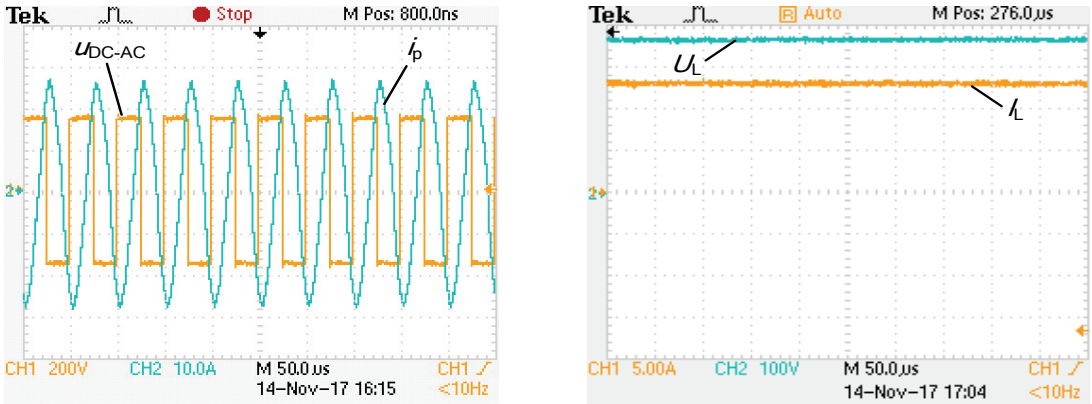

(a) (b)

Fig. 20. Key waveforms of the system.

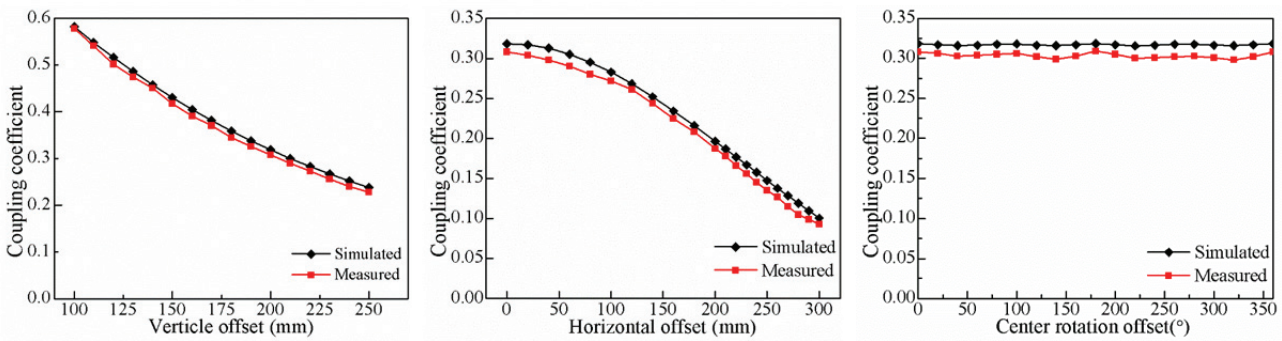

(a) (b) (c)

Fig. 21. Simulated and measured coupling coefficient of the cross-shaped pads prototype against: (a) Vertical offset; (b) Centered rotation offset; (c) Horizontal offset.

216 and a self-inductance of 466.3µH at 20kHz when the air gap is 200mm. The power loss in the transmitter pad is 108.4W and the heat dissipation is only 20.91 mW/cm^2. When compared with the transmitter pad, the receiver is lower due to its lower VA rating. Therefore, the power pads have no obvious temperature rise. A high self-inductance of 466.3µH means that 1.17kV is required across the terminals of the transmitter pad to get a 19.89 ARMS current. This requires careful terminal insulation to avoid a potential hazard. However, with the purpose of effectively reducing both the inductance and the voltage at the external terminals, the compensation capacitors can be placed in series with the pad windings and internal to the pad structures.

Going further, in order to meet the lower voltage limits, the capacitors can be distributed throughout the windings [10], [14]. The graphs in Fig. 21(c) show the simulated and measured coupling coefficient of the cross-shaped pads prototype against a center rotation offset at a 200mm gap. With the receiver pad rotating around the central axis, the coupling coefficient remains constant, which is superior to the DD pads proposed in [14].

The graphs in Fig. 21(b) show that the measured coupling coefficient has a 70% decline when the horizontal offset is 300mm at a 200mm gap. This also leads to a decline in the

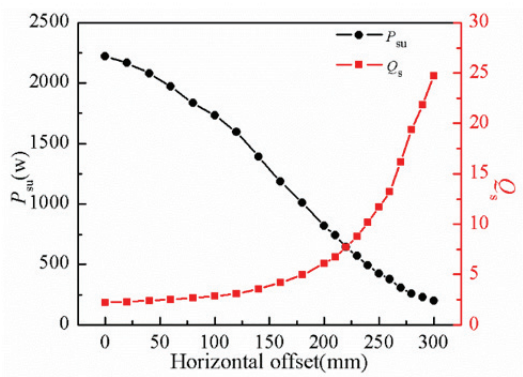

Fig. 22. Measured horizontal profiles (P_{su}) at a 200mm gap with a primary current of 20 ARMS at 20 kHz and the operational Q_s for a 5 kW output.

system transmission capacity. Therefore, an adjustable Q_s is required to make the system output power constant for charging EVs. The graphs in Fig. 22 show measured horizontal profiles (P_{su}) at a 200mm gap with a primary current of 20 ARMS at 20 kHz and the operational Q_s for a 5 kW output.

As is shown, the power transmission capacity of the 200mm gap, 5 kW system descends rapidly with an increase of the horizontal offset. According to equation (1), Q_s with a constraint of 2-10 can be adjusted to meet the needs of a 5 kW

output, according to the component VA ratings and tolerances in practical applications [13]. Assuming a maximum value of 10, a horizontal shifting of 240mm is allowed. However, an increase of the Q_s values leads to lower stability of the secondary side and the extremely high values mean system failure. Meanwhile, an increase of Q_s leads to a lower system efficiency.

A curve showing the system efficiency η with a 0-240mm horizontal offset is shown in Fig. 23. The power loss is mainly located on the inverter power electronics, coil resistance and rectifier. With an increase of the offset, the efficiency is gradually reduced. This is because the current in the secondary pick-up side increases with a higher offset, which leads to greater losses on pick-up pads and rectifier power electronics.

The charge zone for the receiver pad of the cross-shaped pads are shown in Fig. 24. A full 5kW of power can be transferred within the lightly shaded circular areas of the transmitter, with a diameter of Φ=1400mm. That is, a free charging zone of 1.54m^2 is provided for the whole receiver pad with an air gap of 200mm, which is sufficient for parking without supportive electronic devices if appropriate markings are made in the parking areas.

To apply an IPT charging system in an electric vehicle, the power pads should comply with the International Commission on Non-Ionizing Radiation Protection guidelines (ICNIRP). These guidelines are enacted in order to limit human exposure to time-varying electric magnetic fields. According to different effects when the human body is exposed to different frequency electromagnetic waves, the ICNIRP formulates exposure limits in different frequency ranges. Generally, the higher the frequency, the greater the damage. However, sometimes it is harmful when a system resonances at a lower frequency. ICNIRP stipulates that the general public should not be exposed to body average RMS flux densities beyond 6.25μT in the frequency range of 0.8 to 150 kHz. This limit is raised for occupational exposure and is frequency dependent; between 0.8 to 65 kHz the limit is 30.7μT, and between 65 to 150 kHz the exposure level in μT is defined by 2.0/f, where f is the frequency in MHz; this corresponds to 13.3μT at 150 kHz [25]. However, the ICNIRP does not explicitly describe measurement techniques for determining whether systems meet these guidelines. Measurement techniques have been addressed by the Australian Radiation Protection And Nuclear Safety Agency (ARPANSA). These measurement techniques have been based on the ICNIRP guidelines formulating human exposure standards covering frequencies from 3 kHz to 300 GHz [26]. The ARPANSA standard exposure levels are also frequency dependent, and the reference level for the general public and occupational exposure to magnetic fields are 6.1μT between 10 kHz to 65 kHz. These measurement techniques state that the leakage magnetic flux density cannot exceed the spot

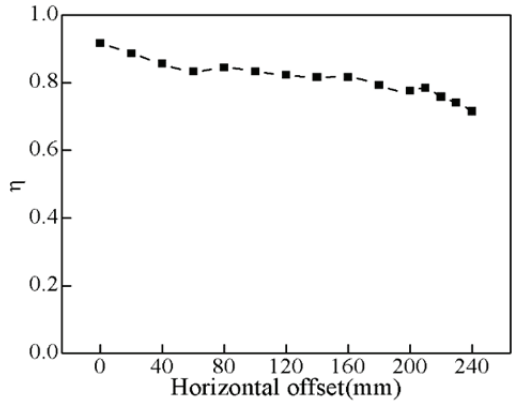

Fig. 23. Relation between the system efficiency and the horizontal offset.

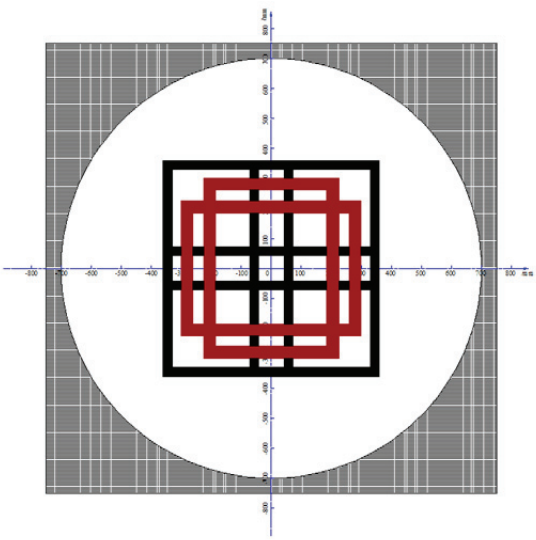

Fig. 24. Charge zone of cross-shaped pads for a 5 kW output at a 200mm gap.

limits or the body average (equal to 6.1μT). The spot limits may be up to a factor of √20 higher than the exposure level at a given frequency. Consequently, the maximum exposure level for the general public at a given spot is 27.3μT in the frequency range of 10 to 65 kHz. The body average is discussed at four points of the human body: knees, groin, chest and head.

The maximum general public spots exposure should not exceed 27.3μT and the body average exposure levels should be lower than 6.1μT for the IPT system presented in this paper. Measurements were taken with a SPECTRAN NF-5035 electromagnetic field radiation tester from AARONIA to investigate the exposure level around the cross-shaped pads with a 100mm offset at a gap of 200mm. The leakage magnetic flux above and below the pads is very low due to the ferrite layers, which will be further replaced by aluminum shielding. The magnetic flux density along the measurement line midway between the pads is shown in Fig. 25. The graphed contour illustrates the worst situation in which the

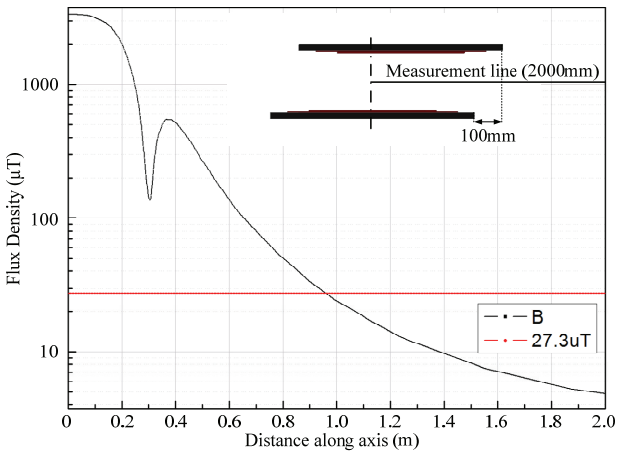

Fig. 25. Leakage magnetic flux density along the measurement line midway between the pads.

leakage magnetic flux exposure level is the greatest in this measurement line. This situation can be improved using aluminum shielding. The peak of curve is 3368μT in the center of the power pads, and the magnetic flux density of 27.3μT is at a distance of 960mm from the pads center. Body average exposure at the four points of knees, groin, chest and head of a 170cm person are separately 10.37μT, 6.83μT, 3.89μT and 2.98μT across a person while standing 1.3m away from the center of the power pads, which complies with the ARPANSA regulations. As a result, some necessary means to test the presence of organisms should be used to prevent animals or humans from entering the excessive exposure areas.

VI. Conclusion

IPT charging systems are safe, convenient and efficient when it comes to electric vehicles and its performance is mainly up to the power pads. The coupling coefficient is an excellent measurement indicator for comparing various power pads designs and can be easily measured by a LCR meter. A novel magnetic coupling structure, referred to as cross-shaped pads, with a high coupling coefficient and high tolerances in vertical and center rotation offset has been proposed. With 3-D magnetic finite-element analysis software, the dimensions and shapes of the core layer and coils of the power pads can be optimized to obtain a higher coupling coefficient. An optimized 5 kW IPT system with 720× 720mm cross-shaped pads at a 200mm air gap is made to verify the presented simulation as well as its characteristics. The 1.54m^2 free charging zone provided by the power pads is large enough to park without the need for any electronic devices if appropriate markings are made in the parking areas. At the same time, the leakage flux density measured by a SPECTRAN NF-5035 electromagnetic field radiation tester is fully compliant the ICNIRP requirements according to the ARPANSA regulations. Consequently, the new cross-shaped power pads proposed in this paper can meet the needs of electric vehicle IPT charging systems and provide more choices for the design of the power pads of IPT systems.

Acknowledgment

This work was supported by Natural Science Foundation of China(No.51777210), Natural Science Foundation of Jiangsu Province(No. BK20171190) and Education & Teaching Innovation Project for Postgraduate of China University of Mining and Technology (YJSJG_2017_053).

References

[1] R.-C. Kuo, P. Rieh, A. Satyamoorthy, W. Plumb, P. Tustin and J. Lin, "A 3D resonant wireless charger for a wearable device and a mobile phone," in *Proc. IEEE Wireless Power Transfer Conference (WPTC)*, pp. 1-3, 2015.

[2] A. Berger, M. Agostinelli, C. Sandner, S. Vesti, and M. Huemer, "High efficient integrated power receiver for a Qi compliant wireless power transfer system," in *Proc. IEEE Wireless Power Transfer Conference (WPTC)*, pp. 1-4, 2016.

[3] T. Campi, S. Cruciani, F. Palandrani, V. D. Santis, A. Hirata, and M. Feliziani, "Wireless power transfer charging system for AIMDs and pacemakers," *IEEE Trans. Microw. Theory*, Vol. 64, No. 2, pp. 633-642, Feb. 2016.

[4] T. Campi, S. Cruciani, V. D. Santis, and M. Feliziani, "EMF safety and thermal aspects in a pacemaker equipped with a wireless power transfer system working at low frequency," *IEEE Trans. Microw. Theory*, Vol. 64, No. 2, pp. 375-382, Feb. 2016.

[5] Y.-W. Bai and G.-Y. Su, "Design of a multi-voltage wireless charging pad for small household electrical appliances," in *Proc. IEEE 5th Global Conference on Consumer Electronics(GCCE)*, pp. 1-2, 2016.

[6] C. Park, S. Lee, S. Y. Jeong, G.-H. Cho, and C. T. Rim, "Uniform power I-type inductive power transfer system with DQ-power supply rails for on-line electric vehicles," *IEEE Trans. Power Electron.*, Vol. 30, No. 11, pp. 6446-6455, Nov. 2015.

[7] T. Hata and T. Ohmae, "Position detection method using induced voltage for battery charge on autonomous electric power supply system for vehicles," in *Proc. 8th IEEE Int. Workshop Adv. Motion Control*, pp. 187-191, 2004.

[8] S. Zhou and C. C. Mi, "Multi-paralleled LCC reactive power compensation networks and their tuning method for electric vehicle dynamic wireless charging," *IEEE Trans. Ind. Electron.*, Vol. 63, No. 10, pp. 6546-6556, Oct. 2016.

[9] M. Park, V. T. Nguyen, S.-D. Yu, S.-W. Yim, K. Park, B. D. Min, and S.-D. Kim, "A study of wireless power transfer topologies for 3.3 kW and 6.6 kW electric vehicle charging infrastructure," in *Proc. IEEE Transportation Electrification Conference and Expo, Asia -Pacific (ITEC)*, pp. 689-692, 2016.

[10] J. Deng, W. Li, T. D. Nguyen, S. Li, and C. C. Mi, "Compact and efficient bipolar coupler for wireless power chargers: design and analysis," *IEEE Trans. Power Electron.*, Vol. 30, No. 11, pp. 6130-6140, Nov. 2016.

[11] K. W. Klontz, D. M. Divan, and D. W. Novotny, "An actively cooled 120 kW coaxial winding transformer for fast charging electric vehicles," *IEEE Trans. Ind. Appl.*, Vol. 31, No. 6, pp. 1257-1263, Nov./Dec. 1995.
[12] M. Budhia, J. T. Boys, G. A. Covic, and H. Chang-Yu, "Development of a single-sided flux magnetic coupler for electric vehicle IPT charging systems," *IEEE Trans. Ind. Electron.*, Vol. 60, No. 1, pp. 318-328, Jan. 2013.
[13] M. Budhia, G. A. Covic, and J. T. Boys, "Design and optimization of circular magnetic structures for lumped inductive power transfer systems," *IEEE Trans. Power Electron.*, Vol. 26, No. 11, pp. 3096-3108, Nov. 2011.
[14] M. Budhia, G. Covic, and J. Boys, "A new IPT magnetic coupler for electric vehicle charging systems," *in Proc. Annu. Conf. IEEE Ind. Electron.*, pp. 2487-2492, 2010.
[15] A. Zaheer, D. Kacprzak, and G. A. Covic, "A bipolar receiver pad in a lumped IPT system for electric vehicle charging applications," in *Proc IEEE Energy Convers. Congr. Expo.,* pp. 283-290, 2012.
[16] A. Zaheer, H. Hao, and G. A. Covic, "Investigation of multiple decoupled coil primary pad topologies in lumped IPT systems for Interoperable electric vehicle charging," *IEEE Trans. Power Electron.*, Vol. 30, No. 4, pp. 1937-1955, Apr. 2015.
[17] H. Feng, T. Cai, S. Duan, J. Zhao, X. Zhang, and C. Chen, "An LCC-compensated resonant converter optimized for robust reaction to large coupling variation in dynamic wireless power transfer," *IEEE Trans. Ind. Electron.*, Vol. 63, No. 10, pp. 6591-6601, Oct. 2016.
[18] C.-Y. Huang; J. T. Boys, G. A. Covic and M. Budhia, "Practical considerations for designing IPT system for EV battery charging," in *Proc. IEEE Vehicle Power and Propulsion Conference*, pp. 402-407, 2009.
[19] O. H. Stielau and G. A. Covic, "Design of loosely coupled inductive power transfer systems," in *Proc. Int. Conference on Power System Technology, (Cat. No.00EX409)*, pp. 85-90, 2000.
[20] A. J. Moradewicz and M. P. Kazmierkowski, "Contactless energy transfer system with FPGA-controlled resonant converter," *IEEE Trans. Ind. Electron*., Vol. 59, No. 2, pp. 945-951, Sep. 2010.
[21] J. Hirai, K. Tae-Woong, and A. Kawamura, "Study on intelligent battery charging using inductive transmission of power and information," *IEEE Trans. Power Electron.*, Vol. 15, No. 2, pp. 335-345, Mar. 2000.
[22] P. Sergeant and A. V. d. Bossche, "Inductive coupler for contactless power transmission," *IET Elect. Power Appl.*, Vol. 2, No. 1, pp. 1-7, Jan. 2008.
[23] Y Matsuda, H. Sakamoto, H. Shibuya, and S. Murata, "A non-contact energy transferring system for an electric vehicle-charging system based on recycled products," *J. Appl. Phys.*, Vol. 99, No. 8, pp.08R902-08R902-3, Apr. 2006.
[24] W. Zhang, J. C. White, A. M. Abraham and C. C. Mi, "Loosely coupled transformer structure and interoperability study for EV wireless charging systems," *IEEE Trans. Power Electron.*, Vol. 30, No. 11, pp. 6356-6367, Nov. 2015.
[25] "Guidelines for limiting exposure to time-varying electric, magnetic, and electromagnetic fields (up to 300GHz)," *Health Phys*., Vol. 74, No. 4, pp. 494-522, Dec. 1998.
[26] Maximum exposure levels to radio frequency fields 3kHz to 300 GHz, Australian Radiation Protection and Nuclear Safety Agency (ARPANSA), 2002.

Siyuan Ren was born in Heilongjiang Province, China, in 1992. He received his B.S. degree in Electrical Engineering from the China University of Mining and Technology, Xuzhou, China, in 2015, where he is presnelty working towards his M.S. degree in the School of Electrical and Power Engineering. His current research interests include power electronics and wireless power transfer.

Chenyang Xia was born in Jiangsu Province, China, in 1982. He received his B.S., M.S. and Ph.D. degrees in Control Theory and Control Engineering from Chongqing University, Chongqing, China, in 2006, 2008 and 2010, respectively. He is presently working as an Associate Professor in the School of Electrical and Power Engineering, China University of Mining and Technology, Xuzhou, China. His current research interests include intrinsic safety switch power supplies and wireless power transfer.

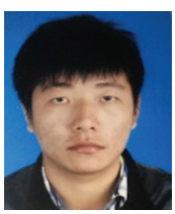

Limin Liu was born in Jiangsu Province, China, in 1992. He received his B.S. degree in Electrical Engineering from the Nanjing University of Information Science and Technology, Nanjing, China, in 2015. He is presently working towards his M.S. degree in the School of Electrical and Power Engineering, China University of Mining and Technology, Xuzhou, China. His current research interests include wireless power transfer.

Xiaojie Wu was born in Hengyang, Hunan Province, China, in 1966. He received his B.S. degree in Industrial Automation, and his M.S. and Ph.D. degrees in Electrical Engineering from the China University of Mining and Technology, Xuzhou, China, in 1988, 1991 and 2000, respectively. From 2002 to 2004, he was a Postdoctoral Researcher at Tsinghua University, Beijing, China. From 1991 to 2016, he was a Professor in the School of Information and Electrical Engineering, China University of Mining and Technology. Since 2016, he has been a Professor in the School of Electrical and Power Engineering, China University of Mining and Technology. His current research interests include the stability of ac machines, advanced control of electrical machines and power electronics.

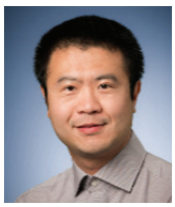

Qiang Yu received his Ph.D. degree from the University of Bundeswehr Muenchen, Munich, Germany, in 2012. From 2008 to 2012, he was an Engineer for FEAAM GmbH, Neubiberg, Germany. From 2013 to 2014, he was a Postdoctoral Research Associate at McMaster University, Ontario, Canada. From 2014 to 2015, he was a Postdoctoral Research Fellow at the Universite Libre de Bruxelles, Brussels, Belgium. He is presently working as an Associate Professor in the School of Electrical and Power Engineering, China University of Mining and Technology, Xuzhou, China. His current research interests include the modeling, design and control of electrical drives and systems.